EVOLUTION IN TEXTURE AND ITS THROUGH-THICKNESS VARIATIONS IN Al-Mg-Si-EXTRUSIONS: EXPERIMENTS AND MODELLING.

Kai Zhang[1], *Knut Marthinsen[2], Bjørn Holmedal[2], Trond Aukrust[3], and Antonio Segatori[1]

[1]Hydro, Innovation & Technology – Europe, Extruded Solutions, 61381 Finspång, Sweden
[2]Department of Materials Science and Engineering, Norwegian University of Science and Technology, NO-7491 Trondheim, Norway
[2]SINTEF Industry, NO-0314 Oslo, Norway

(* Corresponding author: knut.marthinsen@ntnu.no)

ABSTRACT

The visual appearance and mechanical properties of aluminium alloy extrusions are strongly dependent on the microstructure and texture of the extruded profiles, where the desired microstructure and texture may depend on the specific applications. In the present work, the evolution of deformation as well as recrystallization textures during extrusion of AA6xxx aluminium alloys have been experimentally and numerically investigated. Extrusion trials were performed in a laboratory extrusion set-up, which enabled immediate water-quenching of the profiles at the exit of the die, and thus the possibility to capture the deformation texture prior to post-extrusion recrystallization. The textures and their through-thickness variations were experimentally measured by the electron back-scatter diffraction technique (EBSD, and the deformation textures numerically modelled by coupling FEM flow simulations and crystal plasticity (CP) simulations. Different CP models as well as different choices of model parameters were employed and evaluated for texture predictions. With an appropriate choice of crystal plasticity model and model parameters, the deformation texture can mainly be predicted, although the accurate intensities are hard to reproduce. The corresponding recrystallization textures, either generated through spontaneous recrystallization of the extruded profiles or through post-extrusion annealing, are far more challenging to reproduce with available recrystallization models.

KEYWORDS

Al-Mg-Si-alloy, Extrusion, Microstructure, Modelling, Texture

INTRODUCTION

Extrusion is a widely applied thermal-mechanical process to produce aluminium profiles. The properties of the profiles, for example mechanical, fatigue, fracture, corrosion as well surface appearance, are strongly dependent on the underlying microstructure and texture, and the requirements with respect to these aspects may vary with applications (Ralston, et al., 2010; Dumoulin et al., 2012; Donati et al., 2013). Moreover, it is often a challenge to produce extrusions with a consistent and homogenous grain structure and texture along as well as through the cross section of the profiles. It is thus vital to understand and be able to predict (model) how different microstructures and textures are formed and how they evolve during and after extrusion, as basis for controlling the final appearance and properties of extruded profiles.

In the present work, the evolution of deformation as well as recrystallization textures during extrusion of AA6xxx aluminium alloys have been experimentally and numerically investigated. Extrusion trials were performed in a laboratory extrusion set-up, which enabled immediate water-quenching of the profiles at the exit of the die, and thus the possibility to capture the deformation texture prior to post-extrusion recrystallization. The textures and their through-thickness variations were experimentally measured by the electron back-scatter diffraction technique (EBSD) in scanning electron microscopy (SEM).

In order to model the evolution in microstructure texture and its through-thickness variations a model framework has been implemented which includes a FEM model to account for the strain, strain rate and temperature along a set of particle paths during extrusion, which serve as input to an appropriate deformation texture (crystal plasticity) model and a sub-structure evolution model, respectively. The sub-structure model and the crystal plasticity model is in the present work coupled to provide an orientation dependent subgrain size and dislocation density during deformation, which provides the driving force for the post-extrusion recovery and possible recrystallization behaviour at different thicknesses in the profile. The post-extrusion microstructure and texture evolution are calculated with a physically based recovery and recrystallization model, accompanied by a recrystallization texture model.

The framework and its constituent models and their interplay are presented, and the prediction power of this modelling framework is discussed in view of corresponding experimental results.

EXPERIMENTAL

Materials and methods

The main material investigated was an AA6063 alloy (chemical composition in wt% Si 0.4; Mg 0.5; Fe 0.096; Mn 0.017; Ti 0.01; Ga 0.012; Al remaining). After direct chill (DC) casting, the material was homogenized at 580ºC for 135 min, with a heating rate of 250 ºC/h and a cooling rate of 400ºC/h. The grain structure and texture of the billet material were measured by electron back-scattered diffraction (EBSD) in a field emission scanning electron microscope (FESEM) equipped with the TSL orientation imaging microscopy (OIM) software, while the back scatter electron mode (BSE) was used to characterize the second phase particles.

It was found that the initial grains were of equiaxed shape with an average diameter of 90 μm. The texture of the as-cast material was a random texture. The average diameter of the constituent particles was 1.4 μm, whereas the volume fraction was about 0.4%. There were no fine second-phase particles which could retard the recrystallization process.

Billets of 20 mm diameter and 22 mm length were machined from the homogenized material, from which flat profiles of 1.3 mm thickness and 3 mm width were produced by direct extrusion in a laboratory scale direct extrusion set-up. Hence, the average accumulated strain at the end of extrusion was about 4. The container, billet, die and ram were heated together to the testing temperature before the start of extrusion. The results reported in this paper refer to extrusions performed at 350°C and 450°C, respectively, with the same ram speed of 4.5 mm/s. The ram stroke was 9 mm, which accounted for an extrusion time of 2 s. At the end of extrusion, the extrusion material and the die were immediately pushed into cold water while the press ring was retracted. The end of the billet and the profile were quenched below 300°C within 2 s after the end of deformation, reading from the recorded temperature history of an installed thermocouple in the bearing.

The profile extruded at 350°C was cut into small pieces along the extrusion direction (ED). A sample close to the end of the billet was annealed at 480°C for 10 s in a salt-bath, followed by quick water quenching.

For comparison a few additional experiments were carried out on a commercial AA6082 alloy (chemical composition in wt% Si 1.0; Mg 0.7; Fe 0.17; Mn 0.5; Zn 0.01; Al remaining). In this case round billets of 200 mm in diameter were extruded into flat bars of 10 mm thickness and 83 mm in width.

Microstructure and texture characterization

The microstructure of the three as-extruded profiles and the post-extrusion annealed sample was measured by EBSD. The scan was made in the ED - ND plane of the flat profiles (ED: extrusion direction; ND: transverse direction). The scanned areas were positioned very close to the butt-end, where the quenching was fastest and the material flow was close to steady state. The scanned area for the profile extruded at 350 °C was 0.5 mm along ED and 1.3 mm along TD, covering the whole thickness of the profiles, i.e. 1.3 mm along ND. The step size in EBSD for the profile extruded at 350 °C and its post-extrusion annealed counterpart was 1 µm, whereas the step size was 3 µm for the other two profiles.

Recrystallized grains were identified as those being partly or fully surrounded by high-angle boundaries (defined as misorientation angles larger than 15°), with grain size larger than 6 times the scanning step size and a grain orientation spread (GOS) below 2°. The GOS was calculated by first averaging the orientation for each grain. The spread was then obtained by averaging the deviation between the orientation of each point in the grain and the average orientation for the grain. The GOS parameter has been found to be a successful approach with respect to EBSD data to discriminate between recrystallized and deformed grains (Mitsche et al., 2007) Once the recrystallized grains were identified, the recrystallization fraction could be evaluated. The recrystallized grain size is given in terms of the equivalent circle diameter.

The crystallographic texture was analyzed by using all scanning points. ED inverse pole figures (IPF) and ODF (selected sections) were employed to illustrate the texture.

MODELLING

The extrusion microstructure & texture modelling framework implemented and used in this work is schematically illustrated in Fig.1. The constituent models and their interplay are briefly described in the following. The same modelling framework has recently also been applied and evaluated for the extrusion of round profiles of the same alloy (Zhang et al., 2017)

During extrusion each material point in the billet will experience complicated deformation histories, for example strain-rate $\dot{\varepsilon}$, temperature T, pressure, strain ε, etc. will vary at different times t and positions. An accurate description of the deformation history is a prerequisite for a successful modelling framework for predicting the extrusion microstructure and texture. The initial step of the modelling exercise is material flow simulations by FEM, for which the commercial code HyperXtrude has been used. Only steady state extrusion is considered. Deformation history along representative particle paths is output for the subsequent modelling (Aukrust et al., 1997; Zhang et al. 2015b, 2017).

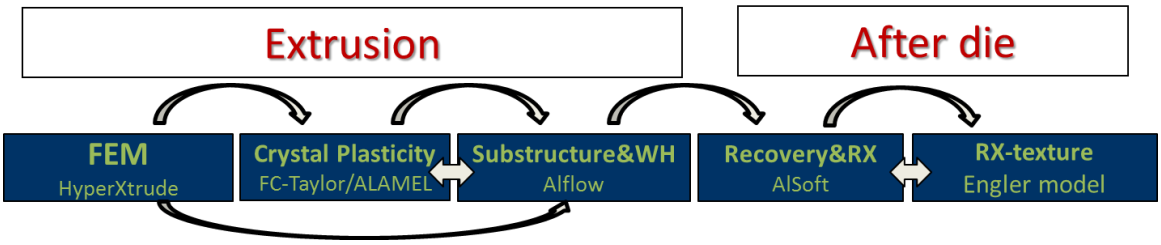

Fig. 1 Scheme of the framework for modelling extrusion microstructures and texture

The deformation microstructure can be characterized by its sub-structure characteristics and texture. Coupling FEM simulations and crystal plasticity (CP) models has recently successfully been applied to give texture predictions similar to the experiments (Zhang et al., 2015a; Zhang et al., 2017). In principle, any CP

model can be used, while advanced CP models such as Alamel-type models have shown to perform better than the FC-Taylor model in predicting the deformation texture. Initial texture and the velocity gradient $\mathbf{L}$ along particle paths from HyperXtrude are the main input to the CP models. The deformation texture simulations are realized by including just conventional octahedral slip as well as with also non-octahedral slip systems included (Maurice & Driver, 1997a, 1997b).

By combining the solution for the dislocation storage problem with models for dynamic recovery of network dislocations and sub-boundary structures, a general internal state variable description is obtained for the sub-structure after deformation, proposed by Nes (1997) and further developed by Nes, Marthinsen and co-workers (2001; 2002). A dedicated version of this model designed for dealing with the problems of work hardening and flow stress saturation in aluminium alloys is referred to as ALFLOW. By coupling FEM and the ALFLOW model, subgrain size δ and cell-interior dislocation density ρ_i at the end of extrusion can be predicted (Marthinsen et al., 2003). Orientation dependent sub-structure properties can also be predicted when coupling ALFLOW with a CP model, which provides the shear rates of slip systems $\dot{\gamma}$ during plastic deformations. The driving pressure (P_D) for the static recrystallization can then be estimated (Vatne et al., 1996a).

The post-extrusion recrystallization behaviour can be calculated by the ALSOFT model. The ALSOFT model is an analytical, statistical approach to predict the combined effect of static recovery and recrystallization during annealing of deformed aluminium (Vatne et al., 1996a; Vatne et al., 1996b; Engler et al., 2007). The deformation microstructure is described by ρ_i and δ, which can be provided by the ALFLOW model. The recovery behaviour, recrystallization kinetics and final recrystallized grain size are the primary output of ALSOFT. The ALSOFT model is based on the assumption of site-saturation nucleation kinetics, and assumes three different nucleation mechanisms, i.e. nucleation from old Cube bands, grain boundary nucleation and particle stimulated nucleation of recrystallization (PSN), from which the total number density of nucleation sites and thus the final grain size can be calculated.

It is currently well accepted that both oriented nucleation and oriented growth control the recrystallization texture. Engler (1997, 1999) has proposed a model for the recrystallization texture based on multiplication of a nucleation probability function and a growth probability function, where the latter is derived from the deformation texture, assuming that only grains having a 40^o <111> orientation relationship with the deformation texture can grow. It is this recrystallization texture model, referred to as the Engler model that is used in the current modelling work. In this model, the probability functions are represented by means of orientation distribution functions (ODF), $f(g)$, where the nucleation mechanisms and their relative contributions can be provided by the ALSOFT model. Alternatively, we have in the present work adopted and tested the ideas of Sidor et al. (2015) that only low stored energy subgrains can act as nucleation sites for recrystallization.

RESULTS

Experimental results

The microstructure of the AA6063 as-extruded profile extruded at T = 350ºC is shown in Fig. 2(a), where the colours are coded according to the ED inverse pole figure (IPF). The as-extruded material for this condition shows a fibrous structure, i.e. a non-recrystallized deformation structure. The right end of the micrograph refers to the centre of the profile, while the left end refers to the surface. Although not easy to see, a more careful quantitative analysis of the substructure, shows that the average sub-grain size decreases somewhat towards the surface, indicating more severe deformation in this region. The texture differences are more obvious (Fig. 2b and c), where we in the centre have a typical plane strain deformation texture (rolling texture), while this texture is distorted towards the surface in the sense that the characteristic rolling texture seems to be 'rotated' around the TD direction (A2 in Figs. 2b and c). The overall texture is quite strong with the Cu-component 22 times random (22R), S 28 times random (28R), Brass 18 times random (18R), while Cube is only 3.4 times random (3.4R).

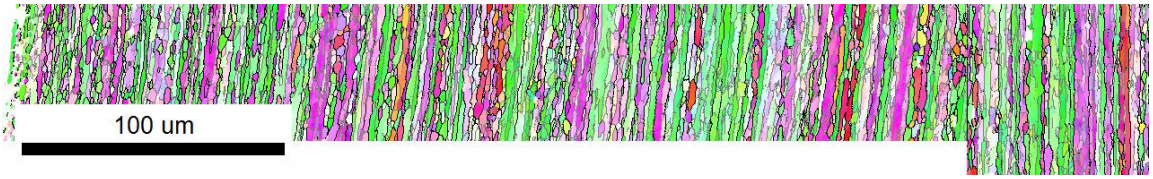

(a)

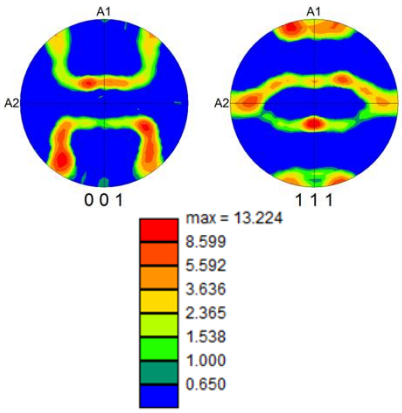

(b)

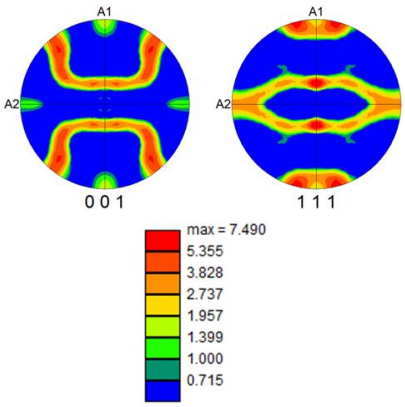

(c)

Fig. 2 (a) IPF grain maps for 350ºC extruded profile, overall scan; (b) Texture, in the form of 001 and 111 pole figures for the centre region, and (c) for the near surface region.

Table 1 Intensity of the beta-fibre texture components and Cube texture in the AA6063 and AA6082 alloys extruded at different temperatures.

Texture component	Copper	S	Brass	Cube	Goss
AA6063@T350	22	28	18	3.4	-
AA6082@T500	13	10	40	23	-

For comparison, the deformation texture of an AA6082 alloy extruded at 500ºC have been recorded, for which a cylindrical billet of diameter 95 mm is extruded into a flat profile of thickness 10 mm and width 80 mm with an extrusion ratio of 12 (corresponding to an average strain of ~2.5). Also this alloy, even at this high extrusion temperature is in a fibrous, non-recrystallized state after extrusion, and can as such be compared with the AA6063 alloy extruded at 350ºC. Although different compositions, the most important difference in this context is the extrusion temperature. The intensities of the main texture components are listed in Table 1. It is interesting to note that the texture is quite different, with the most notable difference the much stronger Cube (23R). The relative intensities for the Copper, S and Brass are also clearly different.

The as-extruded microstructure of AA6063 after extrusion at 450ºC is shown in Fig. 3a and b, in the form of IPF grain maps. In this case the grain structure is a fully recrystallized grain structure, which means that the material spontaneously recrystallized within seconds (< 2s) before/during (water) cooling of the extruded profile. Fig. 3a shows the whole cross-section (RD-ND-section) of the profile from top to bottom surface. It is observed that the bulk of the profile has a fairly equiaxed grain structure (average grain size 23 μm) with a very strong Cube component (89R), some Goss and some ND-rotated Cube. Not so obvious from this example, but what is commonly observed for the extrusion of flat profiles of AA6xxx type alloys is a layer of coarser grains near the surface dominated by the Goss component.

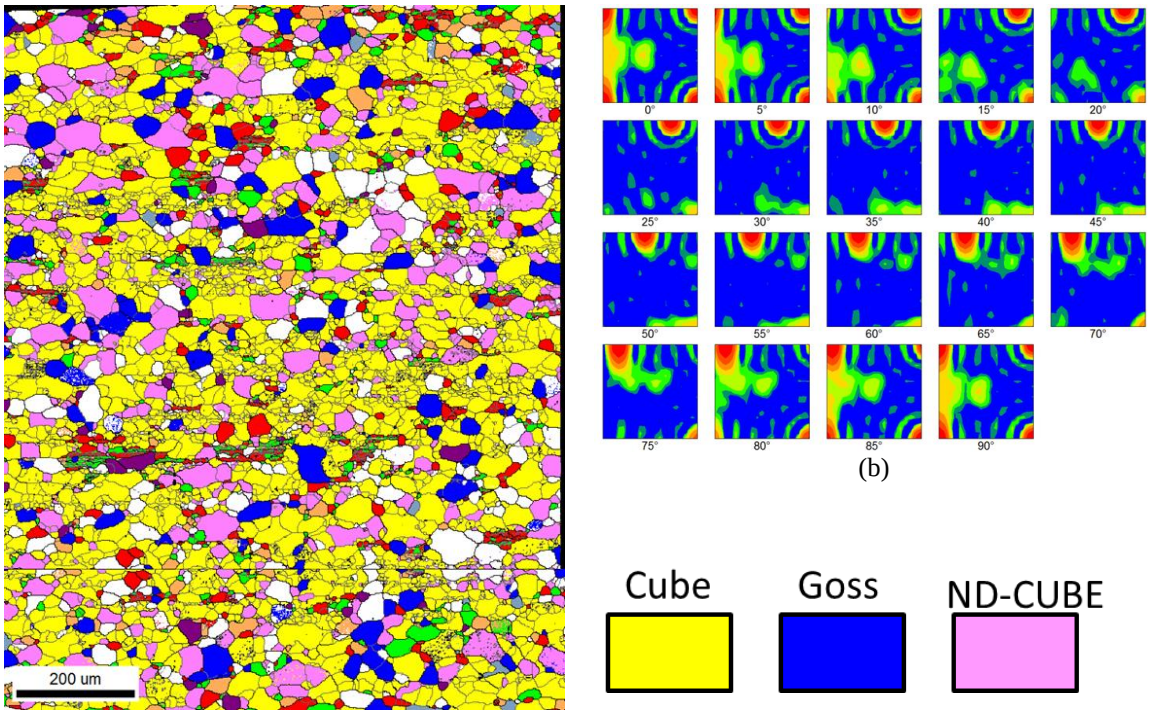

(a) (b)

Fig. 3 AA6063 profile extruded at 450ºC. (a) Through-thickness grain structure of profile. (b) ODF of overall texture (max = 89)

Modelling predictions

The deformation texture was predicted by coupled FEM and CP modelling. Three different CP models have been considered in this work, i.e. the FC-Taylor, the Alamel and the Alamel-Type III model. A description of all the three models can be found in (Zhang et al., 2015a). The FC-Taylor model assumes no grain interaction, whereas the latter two CP models consider grain interaction locally at the grain boundary by introducing relaxations on the strain-constraints. In the first set of trials only conventional octahedral slip were considered, i.e. the twelve {111}<110> slip systems.

The texture prediction was conducted for different particle paths, corresponding to different thickness positions in the profile. The initial texture was assumed to be random and was represented by a total of 8000 random orientations. Following the deformation history for different particle path, from the centre to the surface, the texture at the end of deformation was predicted by the CP models. The predicted results were processed in the TSL OIM software. Same parameters were used when generating the ODFs and the IPFs, as for processing the experimental EBSD data. The predicted textures for the centre path are shown in Fig. 4.

All three models mainly give qualitatively adequate results in the sense that all the main texture components are reproduced, except that for Alamel III, the Brass component has shifted from 35º to 45º in φ_1. However, as observed the relative intensities are not well reproduced. This is even more clearly emphasized by plotting the intensities along the beta-fiber, as illustrated in Fig. 5a. The results show that the Alamel model gives a too weak Brass component, which actually is typical for FC-Taylor type models, while Alamel-III, shows a different trend for the beta-fibre, very different from that of AA6063, but actually closer to AA6082 texture. Compared to AA6063, FC-Taylor apparently performs the best, however, with a too strong Goss component (Cf. Fig. 4b). However, all models predict too little Cube, especially compared to AA6082 deformed at 500ºC. This is problematic in the sense that it is generally accepted that the strong Cube often observed in aluminium alloys during recrystallization of hot deformed Al-alloys, at least partly stems from Cube already present in the deformed conditions (Daaland et al 1996, Vatne at al., 1996a).

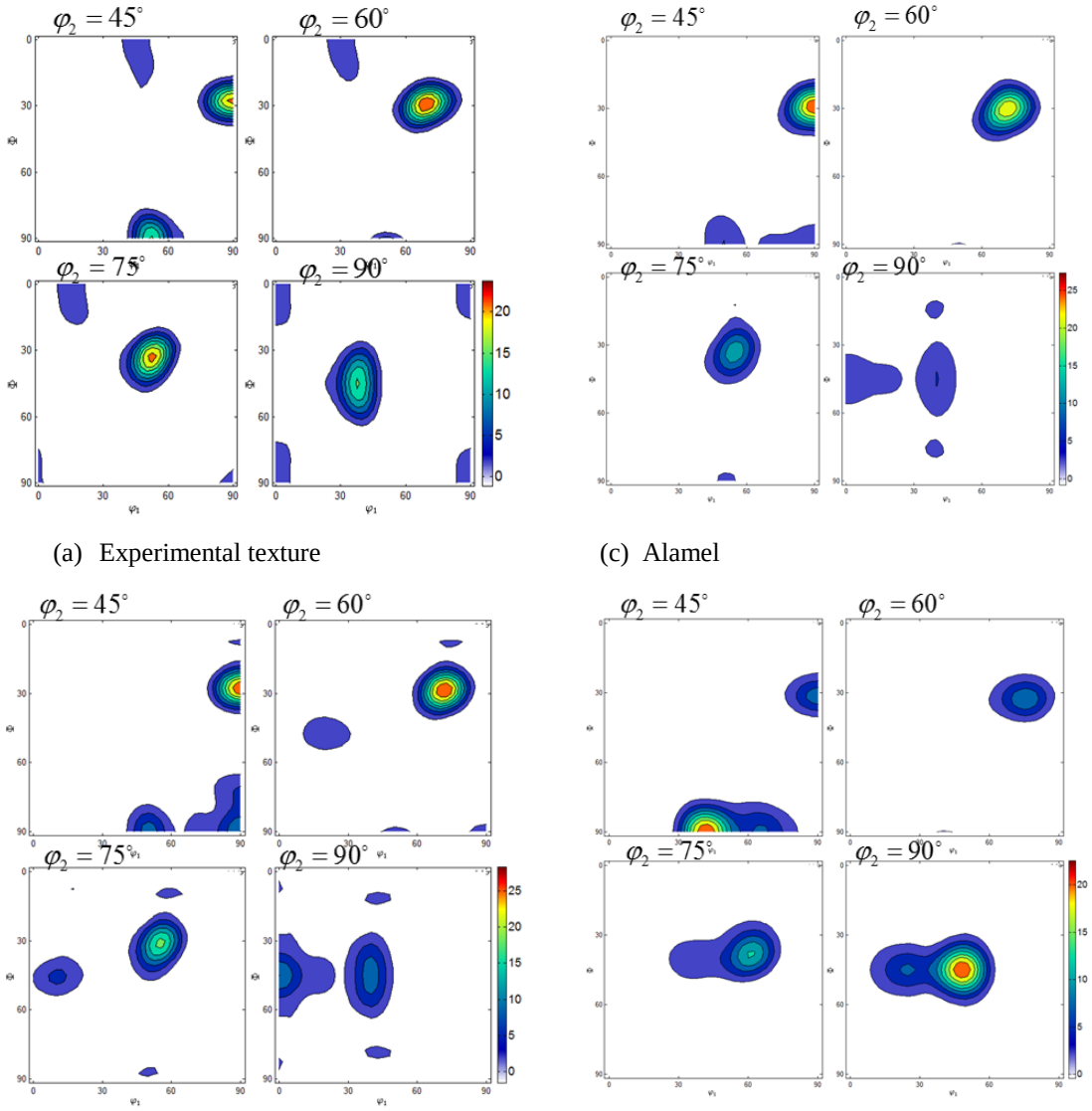

(a) Experimental texture

(c) Alamel

(b) FC Taylor

(d) Alamel III

Fig. 4 (a) Experimental deformation textures for AA6063 extruded at 350ºC, selected sections of the ODF highlighting the main texture components; (b) FC Taylor; (c) Alamel and (d) Alamel III

Maurice & Driver (1997a, 1997b) have shown that non-octahedral slip may play a role at higher deformations temperatures. The deformation texture calculations are therefore repeated, also including non-octahedral slip. The non-octahedral slip systems included in this work are (i) {100}<110>, {112}<110>, {110}<110>, all with the same critical resolved shear stress (CSSR) as for the conventional octahedral slip systems. The resulting results, in terms of the texture intensity along the beta-fibre and predicted Cube intensity are shown in Fig. 5b and in Table 2, respectively. We observe that including non-octahedral slip (most relevant for the AA6082 alloy deformed at 500ºC does increase the Cube intensity, however, still too weak, especially as compared to the AA6082 result. Moreover, the relative intensities along the beta-fibre are still not satisfactory.

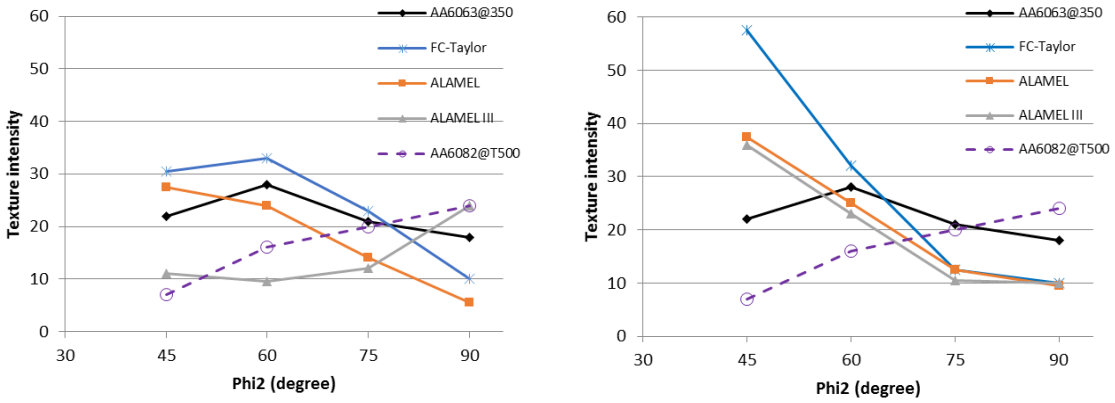

(a) Without non-octahedral slip (b) With non-octahedral slip

Fig. 5 Texture intensity along the beta-fibre for the AA6063 alloy extruded at 350°C and AA6082 extruded at 500°C, and the corresponding model predictions by the FC Taylor, Alamel and Alamel III, respectively. (a) Without non-octahedral slip; (b) with non-octahedral slip.

Table 2 Intensity of the Cube component in extruded AA6063@350 and AA6082@500, and the corresponding texture model predictions without and with non-octahedral slip included in the model calculations.

Cube	AA6063 exp	AA6082 exp	FC Taylor	Alamel	Alamel III
without non-octahedral slip	3.4	23	~1.0	2.5	2.5
With non-octahedral slip			< 1.0	5	9

The capability of the modelling framework to predict the final recrystallization textures is tested for the AA6063 sample extruded at 450°C, which spontaneously recrystallized already during cooling after extrusion. The deformation texture close to the centre and near the surface was calculated by the Alamel CP model, based on the deformation histories provide by the FEM model for the respective deformation paths. Combining the relevant CP model and the ALFLOW model, orientation dependent average sub-grain sizes for the different main texture components (from which the stored energy can be derived) where then calculated and used as basis for the nucleation selection and number density of recrystallization nuclei of different orientation. Here we adopted the ideas of Sidor et al. (2011), where viable recrystallization nuclei are calculated according to

$$\frac{P_D - \min.P_D}{\min.P_{D\min}} \le c \qquad (1)$$

where c is small number much less than one (~ 0.05-01).

Combined with the RX texture model of Engler (1997, 1999) we were able to calculate both the relative number density of different orientations (in this work limited to Cube and Goss) as well the final recrystallization texture. The calculations showed a smaller number of nuclei at the surface, consistent with larger grain size near the surface. Moreover, looking at the final textures shown in Fig. 6, we note that the relative variations of Cube and Goss between centre and surface are qualitatively correct, with a stronger Goss near the surface. However, the strong Cube in centre (and bulk of the profile) is not reproduced, which again reflects that the deformation texture calculations underestimate the Cube in the centre in the deformed state.

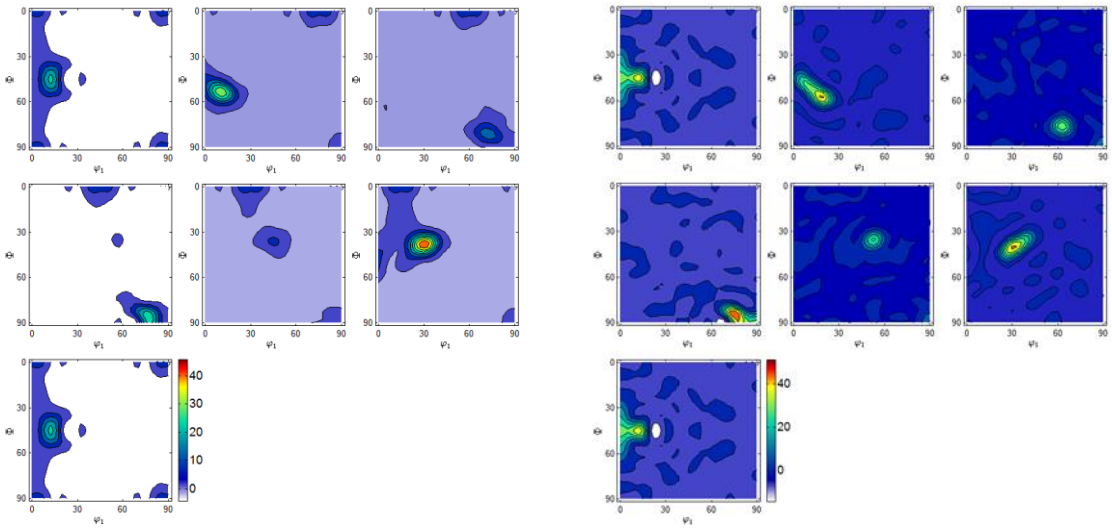

Fig. 6 Calculated recrystallization texture for spontaneously recrystallized AA6063 sample, extruded at 450 ºC. (a) Centre path and (b) Surface path. The ODF is plotted as φ_2 sections, every 15º from 0-90º.

CONCLUSIONS

In the present work, the evolution of deformation as well as recrystallization textures during extrusion of AA6xxx aluminium alloys have been investigated both experimentally and numerically. A physically based modelling framework, previously tested and evaluated for the microstructure and texture evolution in round profiles, has in the present work been applied to predict the texture of laboratory scale flat profiles extruded at 350°C (deformed state) and at 450ºC (already fully recrystallized in the as-extruded state). The deformation texture model predictions are qualitatively correct in the sense that the relevant texture components are captured, however they are not completely satisfactory in quantitative terms as the relative intensities of the main deformation texture components are not well reproduced. In particular, the intensity of the Cube is underestimated by all the different deformation texture models considered. The corresponding recrystallization texture is even more challenging to reproduce, probably partly due to the fact that the deformation textures are not quantitatively well described. However, using the nucleation concept of Sidor et al. (2011, 2015), the trends of the relative through-thickness variations of the Cube and Goss are correct. Although, not perfect, the present through-process modelling framework and its sub-models are promising, but clearly need further improvements, both with respect to quantitative deformation texture predictions as well as with respect to understanding and description of the operating nucleation mechanisms and of the possible subsequent growth selection, for better quantitative predictions of the recrystallization grain size and texture.

ACKNOWLEDGEMENTS

This research work has been supported by the IPN project COSMETEX (228918/O30) in Norway. The financial support by the Research Council of Norway and the industrial partner SAPA AS (Now Hydro Extruded Solutions) is gratefully acknowledged.

REFERENCES

Aukrust, T., Tjøtta, S.,Vatne H.E., & Van Houtte, P. (1997). Coupled FEM and texture modelling of plane strain extrusion of an aluminium alloy, *Int. J. Plast*., 13, 111-125.

Donati, L., Segatori, A., El Mehtedi, M., & Tomesani, L. (2013). Grain evolution analysis and experimental validation in the extrusion of 6XXX alloys by use of a lagrangian FE code, *Int. J. Plast*. 46, 70-81.

Dumoulin, S., Engler, O., Hopperstad, O.S., & Lademo, O.G. (2012). Description of plastic anisotropy in AA6063-T6 using the crystal plasticity finite element method, *Modell. Simul. Mater. Sci. Eng*., 20, 055008.

Daaland, O. & Nes, E. (1996). Recrystallization texture development in commercial Al-Mn-Mg alloys. *Acta mater.* 44, 1413-1435.

Engler, O. (1997). Simulation of the Recrystallization Textures of Al-Alloys on the Basis of Nucleation and Growth Probability of the Various Textures Components, *Textures and Microstruct*., 28, 197-209

Engler, O. (1999). A Simulation of Recrystallization Textures of Al-Alloys With Consideration of the Probabilities of Nucleation and Growth, *Textures and Microstruct.*, 32, 197-219.

Engler O., Lochte L., & Hirsch J. (2007). Through-process simulation of texture and properties during the thermomechanical processing of aluminium sheets. *Acta mater.* 55, 5449-5463.

Holmedal, B., Abtahi, S., Marthinsen, K., & Nes, E. (2002). Modelling the Evolution of Microstructure and Properties during Deformation of Aluminium, *Mater. Sci. Forum*, 396-402, 315-326.

Marthinsen, K., & Nes, E. (2001). Modelling strain hardening and steady state deformation of Al–Mg alloys, *Mater. Sci. Technol.*, 17, 376-388.

Marthinsen, K., Holmedal, B., Abtahi, S., Valle, R., Chen, S. & Nes, E. (2003). Coupled FEM and Microstructure Modeling Applied to Rolling and Extrusion of Aluminium Alloys, Mater. Sci. Forum, 426-432 (2003) 3777-3782.

Maurice, C., & Driver, J.H. (1997a). Hot rolling textures of f.c.c metals – Part I. Experimental results on Al single and polycrystals. *Acta mater*. Vol. 45 (11), 4627-4638.

Maurice, C., & Driver, J.H. (1997b). Hot rolling textures of f.c.c metals – Part II. Numerical simulations. *Acta mater.* Vol. 45 (11), 4639-4649.

Mitsche S., Poelt, P., & Sommitsch C. Recrystallization behaviour of the nickel-based alloy 80 A during hot forming. *J. of Microscopy* 227 267-274.

Nes, E., (1997). Modelling of work hardening and stress saturation in FCC metals, *Prog. Mater Sci.* 41, 129-193.

Nes, E., Marthinsen, K., & Rønning, B. (2001). Modelling the evolution in microstructure and properties during processing of aluminium alloys, J. Mater. Process. Technol., 117, 333-340.

Nes, E., Marthinsen, K., (2002) Modeling the evolution in microstructure and properties during plastic deformation of f.c.c.-metals and alloys – an approach towards a unified model, *Mater. Sci. Eng*. A322, 176-193.

Ralston, K.D., Birbilis, N., & Davies, C.H.J. (2010). Revealing the relationship between grain size and corrosion rate of metals, *Scripta Mater*. 63, 1201-1204 .

Sidor, J., Petrov, R., & Kestens, L. (2011). Modeling the crystallographic texture changes in aluminium alloys during recrystallization. *Acta mater.* 59, 5735-5748.

Sidor, J., Decroos, K., Petrov, R., & Kestens, L. (2015). Evolution of recrystallization textures in particle containing Al alloys after various rolling reductions: Experimental study and modeling. *Int. J. Plast.* 66, 119-137.

Vatne H.E., Furu, T, Ørsund, R., & Nes E. (1996a). Modelling recrystallization after hot deformation of aluminium *Acta mater.* 44, 4463-4473.

Vatne, H.E., Marthinsen, K, Ørsund R, & Nes, E. (1996b) Modeling recrystallization kinetics, grain sizes, and textures during multi-pass hot rolling. *Metall Trans*.27A, 4133-

Zhang, K., Holmedal, B., Hopperstad, O.S., Dumoulin, S., Gawad, J., Van Bael, A., & Van Houtte, P. (2015a) Multi-level Modelling of Mechanical Anisotropy of Commercial Pure Aluminium Plate: Crystal Plasticity Models, Advanced Yield Functions and Parameter. *Int. J. Plast.*, Vol.66, 3-30.

Zhang, K., Marthinsen, K., Holmedal, B., Aukrust, T., & Segatori, A. (2015b) Coupled FEM and Alamel-type Polycrystal Plasticity Modelling Applied to Extrusion of Aluminium Alloys, *Materials Today: Proceedings* 2, 4898-4903.

Zhang, K., Marthinsen, K., Holmedal, B., Friis, J., Pettersen, T. & Segatori, A. (2017). Characterization and Modelling of the Microstructure and Texture Evolution in AlMgSi-Extrusions, *Materials Science Forum*, Vol. 879, 1239-1244.